

Double-finger-gate controlled spin-resolved resonant quantum transport in the presence of a Rashba-Zeeman gap

Chi-Shung Tang,^{1,*} Shu-Ting Tseng,² Vidar Gudmundsson,³ and Shun-Jen Cheng^{2,4,†}

¹*Department of Mechanical Engineering, National United University, Miaoli 36003, Taiwan*

²*Department of Electrophysics, National Chiao Tung University, Hsinchu 30010, Taiwan*

³*Science Institute, University of Iceland, Dunhaga 3, IS-107 Reykjavik, Iceland*

⁴*Physics Division, National Center for Theoretical Sciences, Hsinchu 300, Taiwan*

We investigate double finger gate (DFG) controlled spin-resolved resonant transport properties in an n-type quantum channel with a Rashba-Zeeman (RZ) subband energy gap. By appropriately tuning the DFG in the strong Rashba coupling regime, resonant state structures in conductance can be found that is sensitive to the length of the DFG system. Furthermore, a hole-like bound state feature below the RZ gap and an electron-like quasi-bound state feature at the threshold of the upper spin branch can be found that is insensitive to the length of the DFG system.

PACS numbers: 73.23.-b, 72.25.Dc, 72.30.+q

I. INTRODUCTION

Spintronics utilizing the spin degree of freedom of conduction electrons is an emerging field due to its applications from logic to storage devices with high speed and very low power dissipation.¹⁻³ Manipulating the spin information offers the possibility to scale down certain semiconductor spintronic devices to the nanoscale and is favorable for applications in quantum computing.⁴⁻⁶ Various spin-orbit (SO) effects present in semiconductor structures provide a promising way to spin manipulation in two-dimensional electron gases (2DEG).^{7,8} Particularly, the Rashba SO interaction is of importance in spintronic devices, such as the gate-controllable spin field-effect transistor.⁹⁻¹³

The SO interaction can be induced when the transported electron experiences a strong electric field due to an asymmetry in the confinement potential, namely the Rashba SO interaction is caused by a structure inversion asymmetry (SIA).¹⁴ Especially, the Rashba SO interaction due to SIA can be significantly induced in 2DEG confined by an asymmetric potential in semiconductor materials. Experimentally, the Rashba interaction has been shown to be effective for electron spin manipulation by using bias-controlled gate contacts.¹⁵ Recently, several approaches were proposed to engineer a spin-resolved subband structure utilizing magnetic fields¹⁶⁻²¹ or ferromagnetic materials.^{22,23} The combination of a Rashba SO interaction and an external in-plane magnetic field may modify the subband structure producing a spin-split Rashba-Zeeman (RZ) subband gap feature.^{24,25} To implement a quantum information storing and transfer, not only coherent manipulation¹² but also resonant features involving SO interactions are of importance.²⁶ This can be achieved utilizing a double finger gate (DFG) forming a quantum dot in between the fingers where electrons are subjected to the Rashba SO coupling and the Zeeman interaction.

In this work, we consider a split-gate induced narrow constriction that is fabricated in a 2DEG in a narrow

band gap semiconductor heterostructure. A very asymmetric structure in the 2DEG leads to strong SO coupling with the result that the Rashba effect is dominant. We shall explore spin-resolved quantum transport properties that are manipulated by a double finger gate (DFG) under an external in-plane magnetic field as shown in Fig. 1. Various resonant transport mechanisms in the conductance will be demonstrated analytically and numerically, including resonant states (RS), hole-like bound states (HBS), and electron-like quasi-bound states (EQBS).

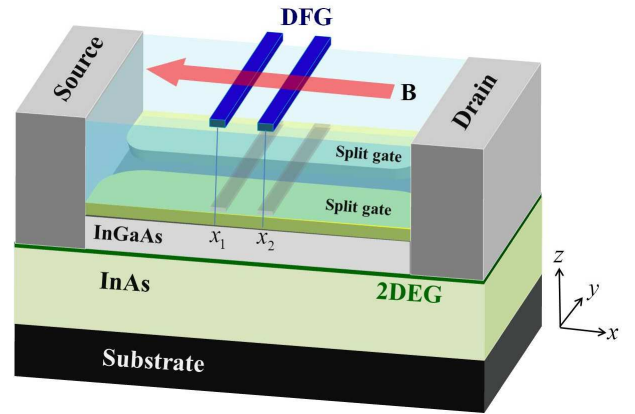


FIG. 1. (Color online) Schematic illustration of the quantum channel device constructed with a 2DEG induced from InAs-In_{1-x}Ga_xAs semiconductor heterostructure. A split-gate is used to control the channel width. An external in-plane magnetic field $\mathbf{B} = B\hat{x}$ ($B < 0$). The DFG is consisted of two finger gates located x_1 and x_2 to influence the spin-resolved resonant quantum transport.

The organization of the rest of this paper is as follows. In Sec. II we describe the propagation-matrix approach of tunneling through a DFG system under in-plane magnetic field. In Sec. III we present our calculated results on the spin-split subband structure and the spin-resolved conductance. A concluding remarks is given in Sec. IV.

II. DFG-CONTROLLED TRANSPORT MODEL

In this section, we shall show how the split-gate confined quantum device influenced by the RZ effect can be describe by a Hamiltonian technique in order to obtain the spin-split subband structures. The corresponding group velocity and effective mass will be obtained to analyze the spin-resolved resonant quantum transport behavior. A propagation matrix approach will be introduced to deal with the DFG-controlled spin-resolved quantum transport.

A. Hamiltonian of the DFG system

As is illustrated for the device in Fig. 1, a two dimensional electron gas (2DEG) is induced in an InAs-In_{1-x}Ga_xAs semiconductor heterojunction grown in the (001) crystallographic direction and is subjected to a split-gate voltage. A pair of split-gates restrict the movement of the electrons of the 2DEG, and therefore a quantum channel is generated in the [100] direction. Propagating electrons in the channel are driven from source to drain.

In the absence of the finger gates, the transported electron is affected by the Rashba effect H_R due to SIA and the Zeeman effect H_Z induced by an external in-plane magnetic field, described by the unperturbed Hamiltonian

$$\tilde{H}_0 = H_0 + H_R + H_Z. \quad (1)$$

The first term describes a bare quantum channel that is described by the ideal Hamiltonian

$$H_0 = \frac{\hbar^2 k^2}{2m^*} + U_c(y). \quad (2)$$

The first term is the kinetic energy of an electron in the 2DEG, where $\hbar = h/2\pi$ is the reduced Planck constant. A conduction electron has an assigned wave number k satisfying $k^2 = k_x^2 + k_y^2$ and m^* is its effective mass. The second term is a confining potential energy modeled by a hard-wall confinement

$$U_c(y) = \begin{cases} 0, & |y| < W/2 \\ \infty, & \text{otherwise,} \end{cases} \quad (3)$$

with W being the width of the quantum channel that can be controlled by applying a split-gate with negative voltage.

In the second term of Eq. (1), we consider a (001) crystallographic 2DEG system, and hence the Rashba SO Hamiltonian $H_R = \alpha(\boldsymbol{\sigma} \times \mathbf{k}) \cdot \hat{\mathbf{z}}$ couples the Pauli spin matrix $\boldsymbol{\sigma}$ to the momentum $\mathbf{p} = \hbar\mathbf{k}$ can be reduced as a k -linear form

$$H_R = \alpha(\sigma_x k_y - \sigma_y k_x), \quad (4)$$

where the Rashba coupling strength α is proportional to the electric field along $\hat{\mathbf{z}}$ direction perpendicular to the

2DEG.¹⁵ The third term in Eq. (1) describes an applied external in-plane magnetic field that is selected to be antiparallel to the channel in the [100] direction and has the form $\mathbf{B} = B\hat{\mathbf{x}}$ ($B < 0$). The longitudinal in-plane magnetic field induced Zeeman term can be expressed as

$$H_Z = g\mu_B B\sigma_x, \quad (5)$$

in which $g = g_s/2$ indicates half of the effective gyromagnetic factor ($g_s = -15$ for InAs) and $\mu_B = 5.788 \times 10^{-2}$ meV/T is the Bohr magneton. In comparison with the Zeeman Hamiltonian H_Z , we may rewrite Eq. (4) in a narrow channel in the form $H_R = g\mu_B B_R\sigma_y$, where the effective Rashba magnetic field $\mathbf{B}_R = B_R\hat{\mathbf{y}} = -\alpha k_x/(g\mu_B)\hat{\mathbf{y}}$. Hence, the spin-resolved quantum channel system without the DFG may be described by the unperturbed Hamiltonian

$$\tilde{H}_0 = H_0 + g\mu_B (B\sigma_x + B_R\sigma_y). \quad (6)$$

In order to manipulate the spin-resolved resonant transport properties, we applied the DFG on top of split gate with an insulator in between, as shown in Fig. 1. We consider that the width of the finger-gate scattering potential, W , should be less than the Fermi wave length $\lambda_F = 31.4$ nm to be described as a delta potential. We consider a high-mobility semiconductor materials so that impurity effects can be neglected. The considered DFG system is then described by the scattering potential energy

$$U_{sc}(x) = e \sum_{j=1}^2 V_j \delta(x - x_j), \quad (7)$$

where V_j indicates the bias potential applied by the finger gate j . The DFG system under investigation is thus described by the Schrödinger equation

$$[\tilde{H}_0 + U_{sc}(x)] \Psi(x, y) = E\Psi(x, y). \quad (8)$$

The eigenfunction $\Psi(x, y)$ in Eq. (8) can be obtained by summing over all occupied subbands, n , for the product of the spatial wave functions and the spin states, given by

$$\Psi(x, y) = \sum_n \phi_n(y) e^{ik_x x} \chi_n. \quad (9)$$

Here the transverse wave function in subband n , of the split-gate induced confining potential energy (3), is of the form $\phi_n(y) = (\pi/W)^{1/2} \sin(n\pi y/W)$ with quantized bare subband energy

$$\varepsilon_{y,n} = \frac{\hbar^2}{2m^*} \left(\frac{n\pi}{W} \right)^2. \quad (10)$$

After some algebra, the corresponding eigenenergies of (8) can be obtained

$$E_n^\sigma(k_x) = \frac{\hbar^2 k_x^2}{2m^*} + \varepsilon_{y,n} + \sigma g\mu_B B_{RZ}, \quad (11)$$

where $\sigma = \pm$ is the spin index, and $B_{\text{RZ}}^2 = B^2 + B_{\text{R}}^2$ is the effective RZ magnetic field with $B_{\text{R}} = 2\alpha k_x / (g\mu_B)$ being a momentum dependent magnetic field due to the Rashba effect. This expression indicates that the subband spin-split energy gap $\Delta E_{\text{RZ}} = E_n^+ - E_n^- = 2g\mu_B B_{\text{RZ}}$ can be changed by tuning the effective RZ magnetic field. It is interesting to note that this spin-split energy gap ΔE_{RZ} is reduced to $\Delta E_Z = 2g\mu_B B$ in the zero momentum limit.

For simplicity, we employ the Fermi-level in a 2DEG as an energy unit, namely $E^* = E_F = \hbar^2 k_F^2 / 2m^*$ with m^* and \hbar being, respectively, the effective mass of an electron and the reduced Planck constant. In addition, one selects the inverse wave number as a length unit, namely $l^* = k_F^{-1}$. Correspondingly, the magnetic field is in units of $B^* = \mu_B^{-1} E^*$, and the Rashba SO-coupling constant α is in units of $\alpha^* = E^* l^*$. In the following we consider a sufficient narrow channel by assuming the channel width $W = \pi l^* = 15.7$ nm so that the bare subband energy due to $U_c(y)$ is simply $\varepsilon_{y,n} = n^2$. The energy dispersion can thus be expressed as

$$E_n^\sigma = k_x^2 + n^2 + \sigma \sqrt{(gB)^2 + (2\alpha k_x)^2}, \quad (12)$$

where $\sigma = \pm$ indicates the upper (+) and lower (-) spin branches. Sufficiently low temperature $k_B T < 0.1\Delta\varepsilon$ or $T < 23$ K is required to avoid thermal broadening effect.

B. Spin-resolved quantum transport

In order to investigate the DFG-controlled spin-resolved quantum transport properties, we shall explore how the spin-mixing effect due to the RZ coupling influences the propagating and evanescent modes for a given energy of an incident electron. The energy dispersion relation (12) can be rewritten in the form

$$k_x^4 - [4\alpha^2 - (K_n^\sigma)^2] k_x^2 + (K_n^\sigma)^2 - (gB)^2 = 0, \quad (13)$$

where $K_n^\sigma = E_n^\sigma - n^2$ indicates the ideal kinetic energy of an electron in the transverse subband n in the absence of a RZ effect. To proceed, one has to label the four longitudinal wave numbers k_x as the right-going k_σ and left-going q_σ , in which the notation $\sigma = +$ indicates spin-up mode and $\sigma = -$ stands for spin-down mode.

Below, we focus on a sufficiently narrow quantum channel to explore the first two conductance steps associated with the two spin branches of a transported electron occupying the lowest subband. We calculate the quantum transport properties by using a generalized spin-resolved propagation matrix method, in which the spin branches as well as spin-flip scattering mechanisms are taken into account. The energy dispersion shown in Fig. 3(a) essentially divides the energy spectrum into three regimes, namely the low energy regime $E_{\text{bottom}}^- < E < E_{\text{top}}^-$, the intermediate energy regime $E_{\text{top}}^- < E < E_{\text{bottom}}^+$, and the high energy regime $E > E_{\text{bottom}}^+$. In the low and high energy regimes, there are four propagating modes with real

k_σ and real q_σ . It should be noted that there are two propagating and two evanescent modes in the intermediate energy regime or the RZ energy gap region where the evanescent modes manifest a bubble behavior with imaginary wave vectors.¹²

The spin-resolved wave functions around the scattering potential U_{sc} located at x_j given by Eq. (7) can be formally expressed as

$$\psi(x) = \sum_{\sigma=\pm} A_\sigma e^{ik_\sigma x} \chi(k_\sigma) + \sum_{\sigma=\pm} B_\sigma e^{iq_\sigma x} \chi(q_\sigma), \quad x < x_j \quad (14)$$

$$\psi(x) = \sum_{\sigma=\pm} C_\sigma e^{ik_\sigma x} \chi(k_\sigma) + \sum_{\sigma=\pm} D_\sigma e^{iq_\sigma x} \chi(q_\sigma), \quad x > x_j \quad (15)$$

where A_σ and C_σ indicate the right-going wave amplitude corresponding to k_σ , while B_σ and D_σ represents the left-going wave amplitude corresponding to q_σ , and χ_σ stands for the momentum dependent spin states. It is possible to obtain the propagation matrix equation by matching suitable boundary conditions as shown below around the free space or the scattering potential induced by the finger gates, namely the electronic wave function is continuous

$$\psi(x_j^-) = \psi(x_j^+) \quad (16)$$

and the derivative of wave function is discontinuous by a deduction of delta scattering potential energy, given by

$$\psi'(x_j^-) = \psi'(x_j^+) - eV_j \psi(x_j^+). \quad (17)$$

Before matching the above boundary conditions, it is convenient to define the reflection coefficient $r_{\sigma_i, \sigma_f} = B_{\sigma_f} / A_{\sigma_i}$ and the transmission coefficient $t_{\sigma_i, \sigma_f} = C_{\sigma_f} / A_{\sigma_i}$ that involves the spin flip states ($\sigma_i \neq \sigma_f$) and spin non-flip states ($\sigma_i = \sigma_f$). Taking into account the possible incident spin states σ and $\bar{\sigma}$ allows us to write the propagation matrix equation (PME) in terms of the total propagation matrix \mathbf{P}^T

$$\begin{bmatrix} 1 & 0 \\ 0 & 1 \\ r_{\sigma, \sigma} & r_{\bar{\sigma}, \sigma} \\ r_{\sigma, \bar{\sigma}} & r_{\bar{\sigma}, \bar{\sigma}} \end{bmatrix} = \mathbf{P}^T \begin{bmatrix} t_{\sigma, \sigma} & t_{\bar{\sigma}, \sigma} \\ t_{\sigma, \bar{\sigma}} & t_{\bar{\sigma}, \bar{\sigma}} \\ 0 & 0 \\ 0 & 0 \end{bmatrix}. \quad (18)$$

To proceed, we match the wave functions Eq. (14) and Eq. (15) using the boundary conditions Eq. (16) and Eq. (17) corresponding to $U_{\text{sc}}(j)$, and then we rearrange these equations into a 4×4 interface propagation matrix $\mathbf{P}^\delta(j)$ of the delta scattering potential j . Moreover, one has to construct a spin-resolved free-space propagation matrix $\mathbf{P}^F(L)$ with length L between the finger gates, given by $\mathbf{P}^F(L) = \exp(-ik_{i,j}L)\delta_{i,j}$, in which $k_{1,1} = k_\sigma$, $k_{2,2} = k_{\bar{\sigma}}$, $k_{3,3} = -q_\sigma$, and $k_{4,4} = -q_{\bar{\sigma}}$. The total propagation matrix \mathbf{P}^T thus consists of the matrices for the first and second scattering delta potentials $\mathbf{P}^\delta(1)$ and $\mathbf{P}^\delta(2)$ induced by the DFG as well as a free space propagation matrix $\mathbf{P}^F(L)$ between them, given by

$$\mathbf{P}^T = \mathbf{P}^\delta(1)\mathbf{P}^F(L)\mathbf{P}^\delta(2). \quad (19)$$

Solving the PME numerically, we may obtain the reflection and transmission coefficients of the scattering intermediate and final states in the presence of the DFG.

We consider an electron injected from the left reservoir (source electrode) and transported to the right reservoir (drain electrode) for a given incident energy. Solving for the spin non-flip and flip reflection coefficients $r_{\sigma,\sigma}$ and $r_{\sigma,\bar{\sigma}}$, as well as the spin non-flip and flip transmission coefficients $t_{\sigma,\sigma}$ and $t_{\sigma,\bar{\sigma}}$, we can calculate numerically the conductance based on the Landauer-Büttiker framework^{27,28}

$$G = G_0 \sum_{\sigma_L, \sigma_R} \frac{v_{\sigma_R}}{v_{\sigma_L}} |t_{\sigma_L, \sigma_R}|^2. \quad (20)$$

Here $G_0 = e^2/h$ is the conductance quantum per spin branch, and σ_L and σ_R indicate, respectively, the spin branches of the incident and transmitted waves in the left and right leads. Therefore, v_{σ_L} and v_{σ_R} represent the group velocity of corresponding modes in the left and right reservoirs, respectively.

III. NUMERICAL RESULTS

Calculations presented below are carried out under the assumption that the electron effective mass $m^* = 0.023m_0$, which is appropriate for the InAs-In_{1-x}Ga_xAs semiconductor interface with the typical electron density $n_e \sim 10^{12} \text{ cm}^{-2}$.¹⁵ Accordingly, the energy unit is $E^* = 66 \text{ meV}$, the length unit $l^* = 5.0 \text{ nm}$, the magnetic field unit $B^* = 1.14 \text{ kT}$, and the spin-orbit coupling parameter is in units of $\alpha^* = 330 \text{ meV}\cdot\text{nm}$. In addition, the bias potential of the finger gate is in units of $V^* = 330 \text{ mV}\cdot\text{nm}$. By using the above units, all physical quantities presented below are dimensionless.¹²

A. Subband structures with Rashba-Zeeman effect

It is known that the presence of an in-plane magnetic field may split the spin degenerate parabolic energy dispersion vertically toward the higher and lower energy and manifests an energy difference $\Delta E_Z = 2gB$, as shown by black dotted line in Fig. 2. In addition, the Rashba SO coupling may let the subband structure shift horizontally toward the positive and negative momentum directions.

By appropriately tuning the applied in-plane magnetic field, the Rashba SO interaction can be separated into several coupling regimes.

In the intermediate Rashba coupling regime $2\alpha^2 = gB$, the spin-up branch is still parabolic while the spin-down branch manifests a flat subband bottom and $\Delta E_{RZ} = \Delta E_Z$, as shown by red dashed line in Fig. 2. In the strong Rashba coupling regime $gB < 2\alpha^2 \leq 4gB$, the combination of the Rashba and Zeeman interactions provide a possibility to generate a RZ gap with a significant subband in the spin-down branch, as shown by green dash-dotted line in Fig. 2. A significant zero point energy of

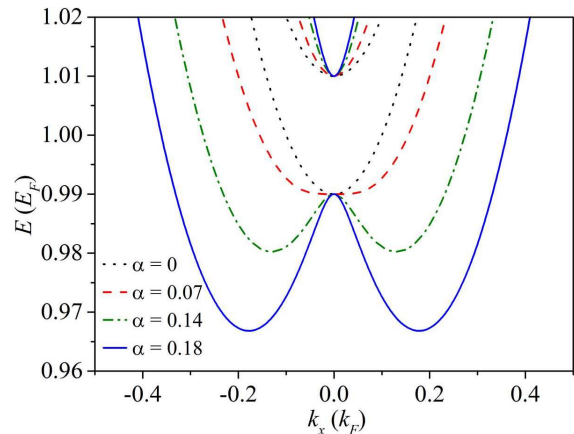


FIG. 2. (Color online) Subband structure in the presence of Rashba-Zeeman interaction under an in-plane magnetic field $gB = 0.01$ for the Rashba coefficients $\alpha = 0$ (black dot), 0.07 (red dash), 0.14 (green dash dot), and 0.18 (blue solid).

a transported electron in the DFG system occurs at the subband top of the spin-down branch. Furthermore, we shall show below that, in the ultra-strong coupling regime $\alpha^2 > 2gB$, the zero point energy will be changed to the subband bottom of the spin-down branch.

In Fig. 3(a), we show the energy dispersion of the first subband with the Rashba coefficient $\alpha = 0.2$ and an in-plane magnetic field $gB = 0.015$. This is within the strong Rashba coupling regime, $2\alpha^2/(gB) > 1$. The subband bottom of the upper spin branch is at $E_{\text{bottom}}^+ = 1 + gB$. However, the subband bottom at $k_x = 0$ of the lower spin branch becomes a subband top with the same energy $E_{\text{top}}^- = 1 - gB$. Therefore, the RZ energy gap of the plus and minus branches ΔE_{RZ} is exactly the Zeeman energy ΔE_Z .

In order to explore the spin-resolved transport properties, it is important to define the group velocity of an electron in the σ spin branch

$$v_\sigma = \frac{dE_n^\sigma}{dk_x} = 2k_x + \sigma \frac{4\alpha^2 k_x}{\sqrt{(gB)^2 + 4\alpha^2 k_x^2}} \quad (21)$$

as shown in Fig. 3(b). Defining the velocity allows us to determine a local minimum and a maximum in the subband structures by setting the group velocity identically zero. We see that there are two subband bottoms in the lower spin branch at $k_x = \pm [\alpha^2 - (gB/2\alpha)^2]^{1/2}$ with the same energy $E_{\text{bottom}}^- = 1 - [\alpha^2 + (gB/2\alpha)^2]$.

To identify an electron-like ($m^* > 0$) and a hole-like ($m^* < 0$) nature, it is necessary to define the effective mass by performing second derivation of energy band, given by

$$\frac{1}{m_\sigma^*} = \frac{d^2 E_n^\sigma}{dk_x^2} = 2 + \sigma \frac{4\alpha^2 (gB)^2}{[(gB)^2 + (2\alpha k_x)^2]^{3/2}}. \quad (22)$$

This expression allows us to define hole-like bound states

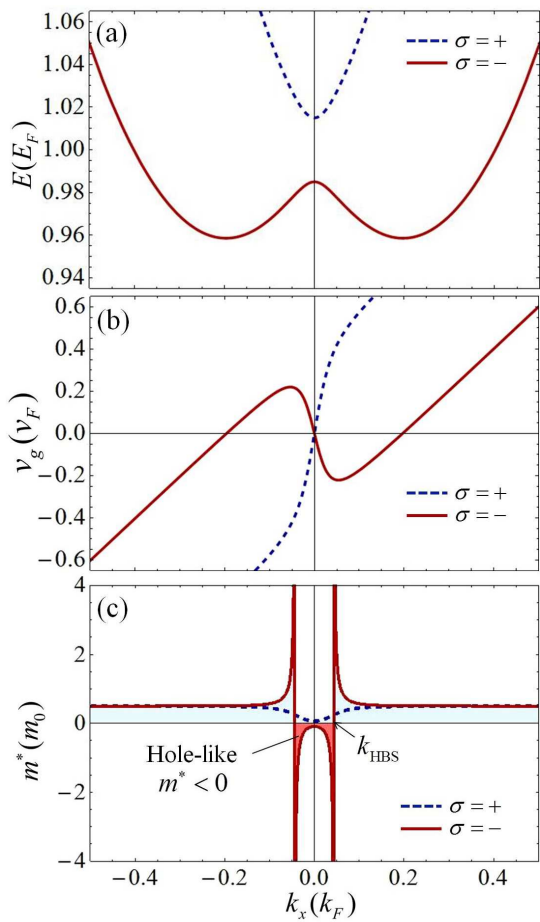


FIG. 3. (Color online) (a) The first spin-split subband structure with Rashba coefficient $\alpha = 0.2$ and magnetic field $gB = 0.015$. The spin-up branch (blue dash) is parabolic while the spin-down branch (red solid) manifests a top and two bottoms of the same energy. (b) Corresponding group velocity of spin-up (blue dash) and spin-down (red solid) branches. (c) Corresponding effective mass in momentum space. The effective mass of a spin-up electron is always positive (blue dash). However, the effective mass of spin-down electron is positive for large wave number k (blue shadow) but is negative for small k (red shadow) due to the strong RZ effect.

(HBS) that occurs when the effective mass goes to infinity, as shown in Fig. 3(c). The corresponding HBS wave number can be analytically expressed as

$$k_{\text{HBS}} = \sqrt{\left| \left[\frac{(gB)^2}{4\alpha} \right]^{2/3} - \left(\frac{gB}{2\alpha} \right)^2 \right|}. \quad (23)$$

The fact that k_{HBS} goes to zero if $2\alpha^2 = gB$ implies the HBS feature can be found only in the strong Rashba coupling regime $2\alpha^2 > gB$.

It is clearly shown in Fig. 3(c) that the effective mass is always positive in the spin-up branch (blue dashed line) while the effective mass in the spin-down branch (red solid line) is allowed to be negative in the small momen-

tum regime $|k_x| < k_{\text{HBS}}$ (red shadow). The corresponding HBS energy can be obtained as

$$E_{\text{HBS}} = 1 - \left(\frac{gB}{2\alpha} \right)^2 + \left[\frac{(gB)^2}{4\alpha} \right]^{2/3} - \left[2\alpha^2 (gB)^2 \right]^{1/3} \quad (24)$$

to investigate the HBS in the conductance as we shall demonstrate in the next section. Having a finite group velocity but an infinite effective mass implies that the electron will be restricted to the energy level corresponding to the inflection point in energy. This is recognized as a HBS in the lower spin branch. The HBS nature will significantly influence the spin-resolved resonant quantum transport behavior.

B. DFG controlled transport

In this section, we discuss how the conductance is influenced by the DFG to manifest various electron-like and hole-like peak structures due to the presence of the RZ coupling. The length L between the two finger gates is tuned to demonstrate these spin-resolved quantum transport features.

Figure 4 shows the spin-split energy dispersion and its corresponding influence on the conductance. Obvious are the peaks corresponding to the resonant ground state in low energy regime and the first excited state in the high energy regime. In Fig. 4(a), we show the spin-split energy dispersion by taking the Rashba coefficient $\alpha = 0.2$ (66 meV nm) and $gB = 0.02$ ($B = 3$ T) to ensure that the system is in the strong SO coupling regime ($2\alpha^2 > gB$). The upper spin branch E^+ manifests a single band bottom $E_{\text{bottom}}^+ = \varepsilon_{y,1} + gB = 1.02$. The lower spin branch E^- exhibits a single band top at energy $E_{\text{top}}^- = \varepsilon_{y,1} - gB = 0.98$ and two band bottoms with the same energy $E_{\text{bottom}}^- = \varepsilon_{y,1} - [\alpha^2 + (gB/2\alpha)^2] = 0.958$.

In Fig. 4(b), we demonstrate how the transport properties are affected by the applied DFG by fixing the finger gate voltage $V_1 = V_2 = 0.6$ while tuning the length L between the two finger gates. In the low kinetic energy regime $E_{\text{bottom}}^- < E < E_{\text{top}}^-$, there are two different resonant features in conductance. The first resonant feature at a lower energy is a resonant state (RS) due to multiple scattering between the two finger gates. When the transported electron is in the double scattering potential induced by the finger gates, it is quasi located in an imaginary quantum well embedded in the quantum channel. The m th RS states are sensitive to the length L between the finger gates and can be approximately estimated by the theoretical formula

$$E_{\text{RS},m}^{\text{th}} = E_{\text{zero}} + \varepsilon_{x,m}, \quad (25)$$

in which $\varepsilon_{x,m} = (m\pi/L)^2$ is the m th energy level due to the DFG with zero point energy E_{zero} . When the Rashba coupling strength is within the ultra-strong coupling regime $\alpha^2 > gB$ as shown in Fig. 4, the zero point

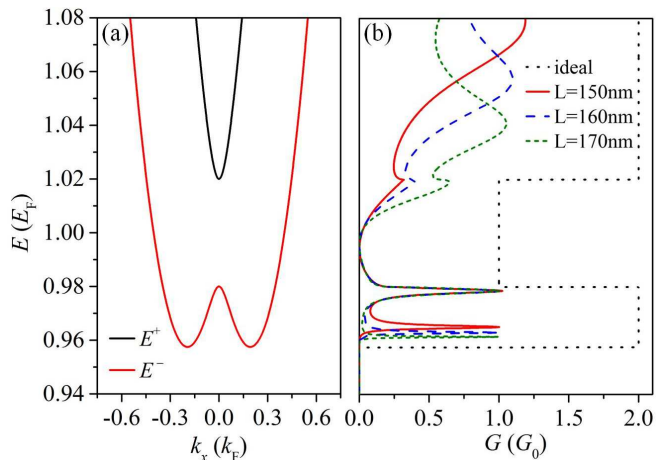


FIG. 4. (Color online) (a) Energy dispersion and (b) corresponding conductance as a function of incident electron energy with different length L between the two finger gates. The ideal case without DFG is shown by black dotted line. The distance between the gate fingers L is selected as 150 nm (red solid), 160 nm (blue dashed), 170 nm (green short dashed). Other parameters are $\alpha = 0.2$, $gB = 0.02$, and $V_1=V_2=0.6$.

energy E_{zero} is identically the subband bottom of the spin-down branch E_{bottom}^- . Theoretically, the first RS structures in conductance are at $E_{\text{RS},1}^{\text{th}} = E_{\text{bottom}}^- + \varepsilon_{x,1} = 0.968, 0.966, 0.965$ for $L = 150, 160, 170$ nm, respectively. In Fig. 4(b), the numerical calculation by means of propagation matrix method gives $E_{\text{RS},1} = 0.965, 0.963, \text{ and } 0.961$ for $L = 150, 160, 170$ nm, respectively. To estimate the accuracy of our theoretical estimation, we define the mean absolute percentage error (MAPE) in energy as

$$M = \frac{100\%}{n} \sum_{i=1}^n \left| \frac{E_{L_i} - E_{L_i}^{\text{th}}}{E_{L_i}} \right|, \quad (26)$$

where n is the number of selected lengths L_i of the DFG system. This formula gives the MAPE of the RS structure in conductance to be $M_{\text{RS},1} = 0.36\%$. Similarly, the theoretical estimation of the fourth RS structures in the conductance are $E_{\text{RS},4}^{\text{th}} = E_{\text{bottom}}^- + \varepsilon_{x,4} = 1.118, 1.098, 1.082$ for $L = 150, 160, 170$ nm, respectively. In the high kinetic energy regime $E > E_{\text{bottom}}^+$, we can find RS peaks in the conductance at $E_{\text{RS},4} = 1.078, 1.057, \text{ and } 1.04$ for $L = 150, 160, 170$ nm, respectively. The MAPE of the fourth RS peak in the conductance is $M_{\text{RS},4} = 3.86\%$.

The transport mechanisms of these conductance peaks are schematically shown by solid blue arrows in Fig. 5. These conductance peaks are associated with resonant bound energy levels $\varepsilon_{x,m}$ and can be tuned by changing the length L between the two finger gates. They will be closer to the lower subband bottom when the length L is increased. We note in passing that the second and the third RS structures $E_{\text{RS},2}$ and $E_{\text{RS},3}$ can not be found in the conductance, these RS features are suppressed due to the formation of the RZ energy gap.

The second resonant feature in the conductance shown

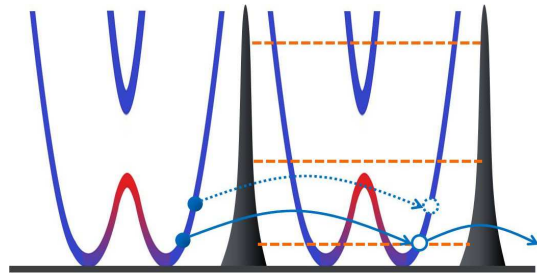


FIG. 5. (Color online) Schematic illustration of resonant state (RS) enhanced transport (solid blue arrow) if the incident electronic energies coincide with the resonant energy levels with zero-point energy at the subband bottom of the spin-down branch, as is shown by broken orange line. However, the electron transmission is not allowed if the incident electron energy is not on the RS shown by the dashed blue arrow.

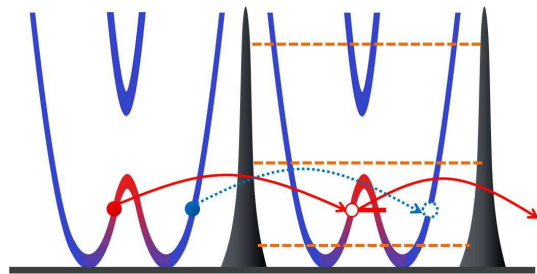


FIG. 6. (Color online) (HBS) Schematic illustration of a hole-like particle transport. The electron transmission is not allowed if the electron energy is not aligned with the resonant state (blue dashed arrow). However, when the electron with incident energy equals the bound state energy of the hole-like subband structure (red solid line), it may contribute to a length insensitive peak structure in conductance (red solid arrow).

in Fig. 4 is a hole-like bound state (HBS) at the same energy $E_{\text{HBS}} = 0.978$ for $L = 150, 160, 170$ nm. The corresponding theoretical prediction based on Eq. (24) is given by $E_{\text{HBS}}^{\text{th}} = 0.972$. The corresponding MAPE is $M_{\text{HBS}} = 0.62\%$. It is found that such HBS structure in the conductance is independent of the distance L between the two finger gates. In the intermediate kinetic energy regime (i.e. in the RZ gap energy regime), a small peak in the conductance can be found at the threshold of the upper spin branch. This structure is recognized as a electron-like quasi-bound state (EQBS). In comparison with the case of a single finger gate system,¹² the EQBS feature is a peak structure instead of dip structure in conductance.

This HBS mechanism is schematically shown by red arrows in Fig. 6 indicating an electron occupying an inner mode in the low kinetic energy regime $E_{\text{bottom}}^- < E < E_{\text{top}}^-$ forming a HBS below the subband top of the spin-down branch. However, the electron with energy E_{HBS} occupying the outer mode is at off-resonant energy and cannot be transmitted through the DFG system, as is

shown by the blue dashed arrows in Fig. 6.

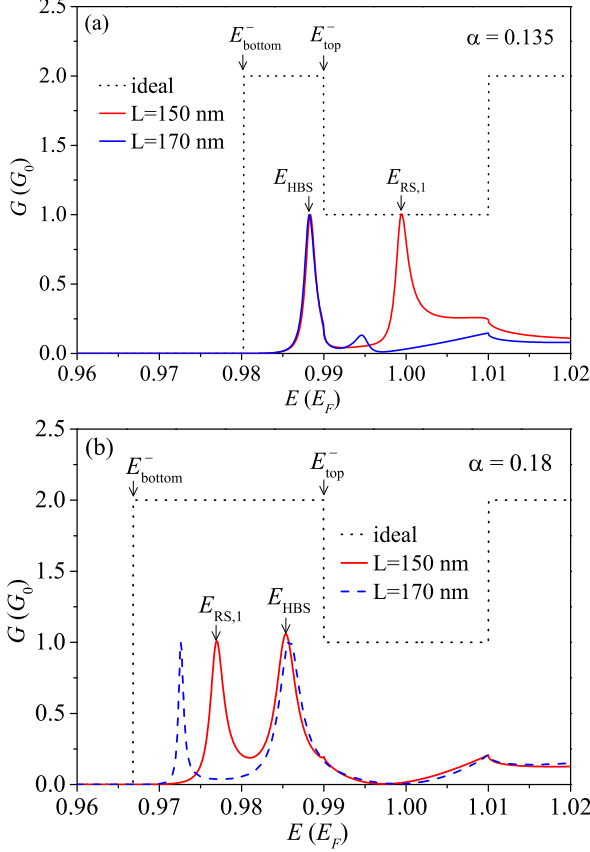


FIG. 7. (Color online) Conductance is plotted as a function of the incident electron energy under magnetic field strength $gB = 0.01$: (a) $\alpha = 0.135$ and (b) $\alpha = 0.18$ with length $L = 150$ nm (red solid) and $L = 170$ nm (blue dash) between the two finger gates. The DFG system is subject to the same positive potential $V_1 = V_2 = 0.6$ in both cases.

In Fig. 7, we show the conductance as a function of energy in an in-plane magnetic field $gB = 0.01$ ($B = 1.5$ T) while tuning the Rashba coefficient to be Fig. 7(a) $\alpha = 0.135$ within the strong coupling regime and Fig. 7(b) $\alpha = 0.18$ within the ultra-strong coupling regime. In both cases, we compare results for the distance $L = 150$ nm (red solid line) and $L = 170$ nm (blue dashed line) between the two finger gates.

In the strong Rashba regime as shown in Fig. 7(a), since the energy difference between the subband top E_{top}^- and the subband bottom E_{bottom}^- of the spin-down branch is small the transported electron occupying the RS manifests a conductance peak at $E_{\text{RS},1}$ satisfying Eq. (25). Our theoretical estimation predicts the zero point energy of the RS peaks in the conductance is at the subband top of the spin down branch, namely $E_{\text{zero}} = E_{\text{top}}^- = 0.9900$. Therefore, we can estimate that the first RS peak in the conductance can be found at energy $E_{\text{RS},1}^{\text{th}} = 1.0000$ and 0.9978 for $L = 150$ and 170 nm, respectively. The numerical result shown in Fig. 7(a) gives $E_{\text{RS},1} = 0.9997$

and 0.9945 for $L = 150$ and 170 nm, respectively. The MAPE of the first RS state $M_{\text{RS},1} = 0.17\%$ in the case of $\alpha = 0.135$ is very accurate.

In the ultra-strong Rashba regime shown in Fig. 7(b), the energy difference between the subband top E_{top}^- and the subband bottom E_{bottom}^- of the spin-down branches become substantial. Therefore, the zero point energy of the first RS peak in the conductance satisfying Eq. (25) will be changed to be $E_{\text{zero}} = E_{\text{bottom}}^- = 0.9668$, and the theoretical estimation of the first RS peak is $E_{\text{RS},1}^{\text{th}} = 0.9768$ and 0.9746 for $L = 150$ and 170 nm respectively. The numerical result shown in Fig. 7(a) gives $E_{\text{RS},1} = 0.9769$ and 0.9726 for $L = 150$ and 170 nm, respectively. The MAPE of the first RS state $M_{\text{RS},1} = 0.11\%$ in the case of $\alpha = 0.18$ is very accurate.

In summary, the above results shown in Fig. 7 demonstrate that when the Rashba coupling is increased from the strong to the ultra-strong regime, the zero point energy of the first RS peak in the conductance will be changed from E_{top}^- to E_{bottom}^- . Furthermore, the RS conductance peak feature can be significantly enhanced. We note in passing that in the intermediate Rashba coupling regime $2\alpha^2 \simeq gB$ (not shown),¹² the zero point energy of the RS peaks will be changed to the subband bottom of the spin-up branch.

IV. CONCLUDING REMARKS

In conclusion, we have investigated the interplay of the Rashba SO coupling and the in-plane magnetic field induced Zeeman effect and its influence on the spin-resolved subband structure forming the Rashba-Zeeman effect induced energy gap. Moreover, we have demonstrated analytically and numerically the subband structure and the spin-resolved resonant quantum transport properties of a DFG system in the presence of a Rashba-Zeeman gap.

Manipulating the DFG system and the Rashba parameter in the strong Rashba regime, $gB < 2\alpha^2 < 4gB$, or in the ultra-strong Rashba coupling regime, $\alpha^2 > 2gB$, allows us to investigate various bound state features. These resonant transport features in the DFG controlled n-type quantum channel include resonant states with various zero point energy in different Rashba coupling regimes, hole-like bound states below the subband top of the spin-down branch, and electron-like quasi-bound states at the threshold of the spin-up branch. Our theoretical findings paving the way for the design of RZ-effect based spintronic device.

ACKNOWLEDGMENTS

This work was supported by the Ministry of Science and Technology, Taiwan through Contract No. MOST 103-2112-M-239-001-MY3, and the National Science

Council, Taiwan under Contracts No. NSC100-2112-M-239-001-MY3, No. NSC-100-2112-M-009-013-MY2, and

No. NSC102-2112-M-009-009-MY2, the Icelandic Research and Instruments Funds, and the Research Fund of the University of Iceland.

-
- * cstang@nuu.edu.tw
 † sjcheng@mail.nctu.edu.tw
- ¹ D. Loss and D. P. Divincenzo, Phys. Rev. A **57**, 120 (1998).
 - ² I. Žutić, J. Fabian, and S. Das Sarma, Rev. Mod. Phys. **76**, 323 (2004).
 - ³ S. A. Wolf, D. D. Awschalom, R. A. Buhrman, J. M. Daughton, S. von Molnár, M. L. Roukes, A. Y. Chtchelkanova, and D. M. Treger, Spintronics: A Spin-Based Electronics Vision for the Future, Science **294**, 1488 (2001).
 - ⁴ *Semiconductor Spintronics and Quantum Computation*, edited by D.D. Awschalom, N. Samarth, and D. Loss (Springer-Verlag, Berlin, 2002).
 - ⁵ D. D. Awschalom and M. E. Flatte, Nat. Phys. **3**, 153 (2007).
 - ⁶ S. Heedt, C. Morgan, K. Weis, D. E. Bürgler, R. Calarco, H. Hardtdegen, D. Grützmacher, and T. Schäpers, Nano Lett. **12**, 4437 (2012).
 - ⁷ R. Winkler, *Spin-Orbit Coupling Effects in Two-Dimensional Electron and Hole Systems*, Springer Tracts in Modern Physics Vol. 191 (Springer, Berlin, 2003).
 - ⁸ L. Meier, G. Salis, I. Shorubalko, E. Gini, S. Schon, and K. Enslin, Nat. Phys. **3**, 650 (2007).
 - ⁹ S. Datta and B. Das, Appl. Phys. Lett. **56**, 665 (1990).
 - ¹⁰ S. Bandyopadhyay and M. Cahay, Appl. Phys. Lett. **85**, 1814 (2004).
 - ¹¹ H. C. Koo, J. H. Kwon, J. H. Eom, J. Y. Chang, S. H. Han, and M. Johnson, Science **325**, 1515 (2009).
 - ¹² C. S. Tang, S. Y. Chang, and S. J. Cheng, Phys. Rev. B **86**, 125321 (2012).
 - ¹³ A. F. Sadreev and E. Ya. Sherman, Phys. Rev. B **88**, 115302 (2013).
 - ¹⁴ E. I. Rashba, Sov. Phys. Solid State **2**, 1109 (1960); Y. A. Bychkov and E. I. Rashba, J. Phys. C **17**, 6039 (1984).
 - ¹⁵ J. Nitta, T. Akazaki, H. Takayanagi, and T. Enoki, Phys. Rev. Lett. **78**, 1335 (1997).
 - ¹⁶ E. R. Mucciolo, C. Chamon, and C. M. Marcus, Phys. Rev. Lett. **89**, 146802 (2002); S. K. Watson, R. M. Potok, C. M. Marcus, and V. Umansky, *ibid.* **91**, 258301 (2003).
 - ¹⁷ A. Brataas, Y. Tserkovnyak, G. E. W. Bauer, and B. I. Halperin, Phys. Rev. B **66**, 60404 (2002).
 - ¹⁸ P. Zhang, Q. K. Xue, and X. C. Xie, Phys. Rev. Lett. **91**, 196602 (2003).
 - ¹⁹ B. G. Wang, J. Wang, and H. Guo, Phys. Rev. B **67**, 092408 (2003).
 - ²⁰ L. Serra, D. Sánchez, and Rosa López, Phys. Rev. B **72**, 235309 (2005).
 - ²¹ M. Scheid, D. Bercioux, and K. Richter, New J. Phys. **9**, 401 (2007).
 - ²² Q. F. Sun, H. Guo, and J. Wang, Phys. Rev. Lett. **90**, 258301 (2003).
 - ²³ W. Zeng, J. L. Wu, B. G. Wang, J. Wang, Q. F. Sun, and H. Guo, Phys. Rev. B **68**, 113306 (2003).
 - ²⁴ Y. V. Pershin, J. A. Nesteroff, and V. Privman, Phys. Rev. B **69**, 121306(R) (2004).
 - ²⁵ C. H. L. Quay, T. L. Hughes, J. A. Sulpizio, L. N. Pfeiffer, K.W. Baldwin, K.W. West, D. Goldhaber-Gordon, and R. de Picciotto, Nat. Phys. **6**, 336 (2010).
 - ²⁶ P. Zhang, Z.-L. Xiang, and F. Nori, Phys. Rev. B **89**, 115417 (2014).
 - ²⁷ R. Landauer, Philos. Mag. **21**, 863 (1970).
 - ²⁸ M. Büttiker, Phys. Rev. B **41**, 7906 (1990).